Bioactive Materials 19 (2023) 690–702

Contents lists available at ScienceDirect

Bioactive Materials

journal homepage: www.keaipublishing.com/en/journals/bioactive-materials

Zinc oxide nanoparticles inhibit osteosarcoma metastasis by downregulating β-catenin via HIF-1α/BNIP3/LC3B-mediated mitophagy pathway

Guanping He [a,c,1], Jing-Jun Nie [b,1], Xiao Liu [c,1], Zihao Ding [a], Peng Luo [b], Yu Liu [c], Bo-Wen Zhang [b], Renxian Wang [b], Xiaoguang Liu [c,***], Yong Hai [a,**], Da-Fu Chen [b,*]

[a] Department of Orthopedics, Beijing Chao-Yang Hospital, Capital Medical University, Beijing, 100020, China
[b] Laboratory of Bone Tissue Engineering, Beijing Laboratory of Biomedical Materials, Beijing Research Institute of Traumatology and Orthopaedics, Beijing Jishuitan Hospital, Beijing, 100035, China
[c] Department of Orthopedics, Peking University Third Hospital, Beijing, 100191, China

ARTICLE INFO

Keywords:
Zinc oxide nanoparticle
HIF-1α/BNIP3/LC3B-mediated mitophagy pathway
Metastasis
Osteosarcoma

ABSTRACT

Osteosarcoma (OS) therapy faces many challenges, especially the poor survival rate once metastasis occurs. Therefore, it is crucial to explore new OS treatment strategies that can efficiently inhibit OS metastasis. Bioactive nanoparticles such as zinc oxide nanoparticles (ZnO NPs) can efficiently inhibit OS growth, however, the effect and mechanisms of them on tumor metastasis are still not clear. In this study, we firstly prepared well-dispersed ZnO NPs and proved that ZnO NPs can inhibit OS metastasis-related malignant behaviors including migration, invasion, and epithelial-mesenchymal transition (EMT). RNA-Seqs found that differentially expressed genes (DEGs) in ZnO NP-treated OS cells were enriched in wingless/integrated (Wnt) and hypoxia-inducible factor-1 (HIF-1) signaling pathway. We further proved that Zn^{2+} released from ZnO NPs induced downregulation of β-catenin expression via HIF-1α/BNIP3/LC3B-mediated mitophagy pathway. ZnO NPs combined with ICG-001, a β-catenin inhibitor, showed a synergistic inhibitory effect on OS lung metastasis and a longer survival time. In addition, tissue microarray (TMA) of OS patients also detected much higher β-catenin expression which indicated the role of β-catenin in OS development. In summary, our current study not only proved that ZnO NPs can inhibit OS metastasis by degrading β-catenin in HIF-1α/BNIP3/LC3B-mediated mitophagy pathway, but also provided a far-reaching potential of ZnO NPs in clinical OS treatment with metastasis.

1. Introduction

Osteosarcoma (OS) occupying the first-place incidence rate in primary bone tumors, is prevalent in 10–20-year-old adolescents characterized with easy recurrence, strong invasion, and early metastasis [1,2]. Although the application of neoadjuvant chemotherapy combined with extensive surgical resection has obviously improved the survival rate of OS patients, there are still some thorny problems, such as drug resistance, strong side effects, and poor survival improvement of patients with metastasis [3,4]. In fact, 10–20% of patients clinically diagnosed with OS develop lung metastasis with a sharp decrease in survival time despite of active treatment [5,6]. Therefore, it is important to explore alternative treatments that can inhibit tumor metastasis and improve the prognosis of OS patients.

In recent years, bioactive nanoparticles (NPs) have gradually become a research hotspot of anti-tumor therapy because of their tumor targeting and superior curative effect, such as silver NPs, copper oxide NPs and iron oxide NPs. Zinc oxide nanoparticles (ZnO NPs), regarded as a "Generally Recognized as Safe" (GRAS) pharmaceutical excipient, are widely used in the biomedical field, such as antibacterial materials and

Peer review under responsibility of KeAi Communications Co., Ltd.
* Corresponding author.
** Corresponding author.
*** Corresponding author.
E-mail addresses: xglius@vip.sina.com (X. Liu), yong.hai@ccmu.edu.cn (Y. Hai), chendafujst@126.com (D.-F. Chen).
[1] These three authors contributed equally to this work.

https://doi.org/10.1016/j.bioactmat.2022.05.006
Received 29 March 2022; Received in revised form 4 May 2022; Accepted 4 May 2022

sunscreen [7]. In recent decade, multitudes of studies also demonstrated that ZnO NPs can selectively inhibit the growth of various tumors, which are expected to replace traditional chemotherapy drugs for clinical tumor treatment [4,8,9]. However, few researches explore the effect and mechanism of ZnO NPs on tumor metastasis.

Autophagy is a normal physiological process that mediates the degradation of intracellular components to maintain intracellular homeostasis, which can be divided into selective and non-selective autophagy [10]. Selective autophagy includes mitophagy, peroxisome autophagy, endoplasmic reticulum autophagy, ribophagy, etc [11]. In general, activation of autophagy in tumor cells enhance resistance to external mutagenic environments, while excessive activation reversely induces cell death [12,13]. In our previous study, we have clarified that ZnO NPs inhibited OS cell proliferation via activating HIF-1 pathway induced mitophagy [14]. However, whether HIF-1 pathway further regulates tumor metastasis still need to be verified.

Among numerous signaling pathways, the pivotal regulatory role of the Wnt pathway has been emphasized in regulating tumor metastasis performance, such as epithelial mesenchymal transition (EMT), migration and invasion [15,16]. Normally, β-catenin, a critical protein in the Wnt pathway, forms a complex with E-cadherin protein expressing in the cell membrane to mediate cell adhesion. However, in tumor cells, it will translocate to the cytoplasm, and eventually enters cell nucleus to combine with the DNA affinity protein lymphoid enhancer factor/T cell factor (LEF/TCF), activating targeted genes that promote tumor metastasis [17,18]. However, whether the Wnt pathway played a key role in ZnO NP-induced tumor metastasis is rarely to be discussed.

Based on above all, we choose OS as a model to evaluate the anti-tumor metastasis properties of bioactive ZnO NPs. Series of in vitro experiments proved that Zn^{2+} released from ZnO NPs could trigger HIF-1 and Wnt pathway activation to inhibit OS cell metastasis by inducing degradation of β-catenin via HIF-1α/BNIP3/LC3B-mediated mitophagy pathway. Meantime, our in vivo results also observed that ZnO NPs combined with targeting the Wnt pathway showed a synergistic effect on OS lung metastasis with good biosafety. In addition, tissue microarray (TMA) of 78 OS patients also detected higher β-catenin expression, which also provided a far-reaching potential in clinical OS treatment with metastasis.

2. Materials and methods

2.1. Cells and cell culture

Two OS cell lines (U2OS and 143B) and human osteoblast cells (hFOB1.19) were purchased from American Tissue Culture Collection (ATCC). OS cells were cultured in Dulbecco's modified Eagle's medium (DMEM) under condition of 5% CO_2 at 37 °C. hFOB1.19 cells were cultivated in a DMEM/Ham's F12 culture medium combined with G418 under condition of 5% CO_2 at 34 °C. All media were added with 10% fetal bovine serum (FBS), 100 IU/ml penicillin, and 100 mg/ml streptomycin.

2.2. Drugs and antibodies

ZnO NPs were purchased from Sigma-Aldrich (St. Louis, MO, USA). $CoCl_2$ and LiCl were purchased from Sigma-Aldrich (St. Louis, MO, USA). YC-1, ICG-001, 3 MA, EDTA and MG132 were purchased from Selleck Chemicals (Houston, TX, USA). FluoZin-3 staining dye was purchased from Invitrogen (Karlsruhe, Germany). Antibodies against N-cadherin, E-cadherin, vimentin, HIF-1α, β-catenin, LC3B, lamin A, tubulin, and glyceraldehyde-3-phosphate dehydrogenase (GAPDH) were purchased from Cell Signaling Technology (Beverly, MA, USA).

2.3. Characterization of ZnO NPs

ZnO NPs were dissolved in ultrapure water at a concentration of 1 mg/ml, and treated under 200 W ultrasonic treatment for different times (2, 5, 10 min). The obtained solutions were captured and dispersions of ZnO NPs were observed under scanning electron microscope (SEM) and evaluated with Zetasizer nano ZS. Transmission electron microscope (TEM) was also performed to further confirm the ZnO NPs morphology. The X-ray diffraction (XRD) pattern of ZnO NPs was further analyzed by X-ray powder diffractometer (Rigaku SmartLab SE), scanning from 5° to 90° at a scan rate of 2°/min.

2.4. CCK-8 experiment

OS cells at a density of 1×10^4 cells/well were inoculated on a 96-cell culture plate, with 100 UL medium in each well, and then subjected to the different treatments after overnight culture. Next, each well was added with 10 μL CCK-8 (KeyGEN, China) reagent for another 2–4 h at 37 °C, and optical density (OD) values were measured at 450 nm by spectrophotometer. Cell viability (%) was calculated according to the following formula: Cell viability (%) = [OD (intervention group)-OD (blank control group)]/[OD (control group)-OD (blank control group)] × 100%.

2.5. Wound healing assay

OS cells at a density of 5×10^4 cells/well were inoculated on 6-well plates, and scratches were created by a 10 μL pipette tip for wound healing assay. Then, the cells were subjected to the different treatments for the designated time points. The scratch distances at different time points were dynamically measured under an inverted microscope to evaluate cell migration ability using the following formula: Cell migration rate (%) = [D (control group)-D (intervention group)]/D (control group) × 100% (D means Distance).

2.6. Invasion assay

Precooled filtered distilled water was used to dilute Matrigel (BD Biosciences) to a concentration of 25 μg/50 μL, and then quickly transferred into the upper chamber with 8 μm size pore for solidification at room temperature (RT). Cells were starved in DMEM medium without FBS overnight, and then transferred into the upper chamber with DMEM mixed with 10% FBS in the lower chamber. After different interventions, 4% polyformaldehyde was added to fix the cells before 0.4% crystal violet staining. Stained cells were counted under an inverted microscope.

2.7. Transcriptome sequencing (RNA-Seq)

Briefly, total RNA was isolated by TRIzol® reagent (Thermo, USA) after 143B OS cell treated with ZnO NPs (15 μg/ml) for 12 h. Then, RNA-Seq was conducted by OE biotech Co., Ltd. (Shanghai, China). The reads containing poly-N and low-quality reads were removed to obtain clean reads, which were then mapped to reference genome by HISAT2. The fragments per kilobase of exon model per million mapped fragments (FPKM) value and the read count of each gene were calculated by Cufflinks and HTSeq-Count, respectively. The threshold of [log2FC]>1 and $p < 0.05$ were identified for significantly differentially expressed genes (DEGs). Enrichment pathways and functions of DEGs were respectively analyzed by KEGG (Kyoto Encyclopedia of Genes and Genomes) database.

2.8. Quantitative real-time PCR (q-PCR)

To verify the effects of ZnO NPs on Wnt signaling pathway related gene mRNA transcription, we performed qPCR on 143B OS cells. 143B OS cells were treated with ZnO NPs for 12 h at a concentration of 15 μg/ml. Then, specific steps in the following were described according to our previous study [14]. The Wnt4, FZD7, β-catenin and c-Myc mRNA levels

were normalized to that of GAPDH. The corresponding primers were synthetized from Sangon Biotech Crop (Shanghai, China) and the corresponding sequences for Wnt4, Frizzled 7 (FZD-7), β-catenin, c-Myc, and GAPDH are as follows: Wnt4 (5-TCGTGTACGCCATCTCTTCG-3) (Forward), (5-CTGACCACTGGAAGCC CTG-3) (Reverse); FZD7 (5-ATATCGCCTACAACCAGACCAT-3) (Forward), (5-AGGAACG GCACGGAGGAA-3) (Reverse); β-Catenin (5-ATGCGTTCTCCTCA-GATGGTGTC-3) (Forward), (5-CAGAATCCAC TGGTGAACCAAGC-3) (Reverse); c-Myc (5-CAGC GACTCTGAGGAGGAACAA-3) (Forward), (5-CCAGCAGAAGGTGATCCAGACT-3) (Reverse); GAPDH (5-CAGCCTCGTCCCGTAGACAA-3) (Forward), (5-GCCGTG AGTGGAG TCATACTG-3) (Reverse).

2.9. Western blot

Total, nuclear, and cytoplasmic proteins were extracted by RAPI, nucleoprotein and cytoplasmic protein extraction kit (Beyotime), respectively. After purification, protein concentrations were quantified by bicinchoninic acid (BCA) protein assay kit. Protein samples (40 μg) were separated using 5%–10% SDS-PAGE at 80–120 V, and then transferred to a nitrocellulose membrane. After blocking with 5% skimmed milk for 1 h, the membranes were incubated with the primary antibodies overnight at 4 °C followed by the secondary antibodies for another 1 h at RT in the dark. Odyssey system (Biosciences, USA) were used to detected and analysis protein expression.

2.10. Immunofluorescence confocal microscope

OS cells at a density of 3×10^4/well were added to the confocal dishes. After adhesion, cells were divided into different groups and treated for 12 h. After treatment, cells were fixed with 4% paraformaldehyde for 15 min, and then infiltrated with 2% Triton X-100 for another 15 min. Then, the antigen was blocked with 5% bovine serum albumin (BSA) at RT for 1 h. The primary antibody with dilution of 1:200 was cultured with cells overnight, and corresponding fluorescent secondary antibody (1:100) was incubated at RT for another 2 h before 4′,6-diamidino-2-phenylindole (DAPI) staining. Finally, images were observed and photographed by laser scanning confocal microscope.

2.11. Co-immunoprecipitation (Co-IP) assay

OS cells at a density of 2×10^7 cells/plate were inoculated on a 10-cm plate. Cells were lysed using radio immunoprecipitation assay (RIPA). After high-speed centrifugation, the cell supernatant was collected and mixed with protein A/G agarose beads in the presence of 0.05% BSA for 2 h. A small portion (1%) of the lysate was taken and levels of β-catenin and LC3B expression were detected by WB. The lysate was incubated with a β-catenin monoclonal antibody at a 1:100 concentration at 4 °C for 12 h, and then protein A/G agarose beads were added and incubated at 4 °C for 4 h before the immunoprecipitation complex was obtained by centrifugation. Finally, precipitates mixed with HIF-1α or LC3B monoclonal antibodies were then analyzed by WB.

2.12. Intervention experiments

2.12.1. Inhibitor intervention experiment

The selected concentrations of the Wnt pathway activator LiCl (10 mM) and inhibitor ICG-001 (10 μM), hypoxia activator $CoCl_2$ (200 μM) and inhibitor YC-1 (100 μM), autophagy inhibitor 3 MA (10 mM), proteasome inhibitor MG132 (100 nM) and zinc ion chelating agent EDAT (1 mM) were pre-incubated with OS cells for 2 h before ZnO NPs treatment. Then, proliferation, migration and invasion were evaluated by CCK-8, wound healing and transwell assays, respectively.

2.12.2. siRNA intervention experiment

Non-targeting siRNA and LC3B targeting siRNA were obtained using the GenOFF siRNA silencing Kit (Ribbio, China), as described in our previous articles. The effect of siRNA LC3B on ZnO NP-induced OS cell proliferation inhibition, LC3B and β-catenin expression were evaluated using CCK-8 and WB assays, respectively. The target sequence of siRNA LC3B as follows: LC3B siRNA-I (accaaaatcccggtgataataga).

2.13. Intracellular Zn^{2+} levels by FluoZin-3 staining

OS cells at a density of 3×10^4/well were added to 24 well plate. After adhesion, cells were divided into different groups with other 12 h treatment. Then, cells were loaded with FluoZin-3 (2 mM) for another 30 min. Then, cells were washed with PBS for 2 times. Images were observed by fluorescence microscope.

2.14. Inductively coupled plasma-mass spectrometry (ICP-MS)

Briefly, OS cells were added into 6-well plates at a density of 5×10^5/well. After overnight culture, cells were treated by different groups for 24 h, and then intracellular Zn^{2+} levels were detected by ICP-MS as described previously [19].

2.15. Nude mouse tibia orthotopic OS model

All animal procedures were performed in accordance with the Guidelines for Care and Use of Laboratory Animals of Beijing Jishuitan Hospital and approved by the Animal Ethics Committee of the Beijing Jishuitan Hospital. Five-week-old blab/c male nude mice (HFK Bio-Technology Co., Ltd, Beijing, China) were raised in the Department of Laboratory Animal Science of Peking University Health Science Center. The mice were randomly divided into the control and treated groups. Each group contained five mice.

To establish the tibia orthotopic OS model, 143B cells with a density of 1×10^6/50 μL PBS were injected into the right tibial medullary cavity. When the tumor volumes reached 100–150 mm^3, ZnO NPs (5 mg/kg; 50 μl) was given by intratumoral injection and ICG-001 (50 mg/kg; 200 μl) intravenously administrated via tail vein every other day. The body weight and tumor volume were recorded every other day according to the formula: $(width^2 \times length)/0.5$. One representative mouse in each group was killed after continuous intervention for another two weeks. Tumor legs, lungs, and important organs (heart, liver, spleen, kidney) were collected, photographed, and weighed followed by formalin fixation for apoptosis, proliferation and biosafety evaluation by tunnel, ki-67 and hematoxylin-eosin (H&E) staining. Lung node numbers were counted by the gross and microscopic observation. Simultaneously, the main organs were also collected (heart, liver, spleen, and kidney) and examined by H&E staining. Finally, the remaining mice in each group continued to be observed and described the survival curve until the day 50 after tumor inoculation.

2.16. Tissue microarray (TMA)

A total of 80 formalin-fixed paraffin-embedded OS specimens were placed in the TMA (two tissues were invalid) and the TMA was purchased from Xi'an Alena Biotechnology Ltd., Co. The expression of β-catenin was detected using an IHC assay with an evaluation criterion as follows: (1) the color development intensity of the cells: no staining was negative [−], light brown was weakly positive [+], brown was moderately positive [++], and chocolate-brown was strongly positive [+++]; (2) the number of positive cells: less than 10% [−], 10–25% [+], between 26% and 49% [++], and more than 50% [+++]). Finally, results of the qualitative and semi-quantitative coloring intensities were obtained by comprehensive evaluation according to the above two results. At least 5–10 high power fields (HPFs) were randomly observed and the corresponding mean values were calculated.

2.17. Statistical analysis

Data were analyzed by GraphPad Prism 9. All values are represented as the mean ± standard deviation (SD). Comparisons between groups were analyzed by Student's t-test and one-way analysis. p value < 0.05 was considered statistically significant (*p < 0.05, **p < 0.01, ***p < 0.001, ****p < 0.0001).

3. Results and discussion

3.1. Characterization of ZnO NPs

We first confirmed the phase ZnO NPs with XRD (Supplementary Fig. S1). The diffraction peaks of ZnO NPs were consistent with the standard PDF card (No: 65–3411), indicating that ZnO NPs were in crystal state and hexagonal structure. As shown in Fig. 1, ZnO NPs showed different dispersion abilities after ultrasonic treatment. We can see that 2 min of ultrasound treatment is not enough to disperse the ZnO NPs (Fig. 1a). According to the SEM observation and particle size distribution (Fig. 1a–c), the ZnO NPs showed best dispersion and particle size distribution after 5 min of ultrasound treatment, and there were no visible changes in the solutions between 5- and 10-min ultrasound treatments (Fig. 1d). TEM images further confirmed the morphology of ZnO NPs after 5 min ultrasound treatment (Fig. 1e). Thus, the 5 min ultrasound treated ZnO NPs were chosen for following in vitro and in vivo experiments.

3.2. Inhibition ability of cell migration and invasion in OS of ZnO NPs

Although many studies have reported the killing effect of ZnO NPs on various tumors [4,8], few studies have systematically explored the effect and mechanisms on tumor metastasis. Our previous research has also confirmed the safety and effectiveness of ZnO NPs on OS growth, which provide a good experimental basis for the application of ZnO NPs in the clinical OS treatment [14,20,21]. However, some chemotherapeutic drugs with definite tumor killing effect have been reported to make tumor cells acquire stronger invasive and metastatic abilities [22], which make it necessary for researchers to further evaluate the metastatic abilities of a new chemotherapy drug with confirmed tumor cell-killing ability. Tumor cell migration and invasion are prerequisites for tumor metastasis, which enable cells to break through vascular endothelial cells into the blood circulation [23]. Therefore, in this study, the effect of ZnO NPs on OS cell migration and invasion were evaluated by wound healing and transwell assay.

We firstly used CCK-8 assay to verify the effect of ZnO NPs on OS proliferation (Supplementary Fig. S2) [20]. Then we selected a low and medium concentration of ZnO NPs on OS cell proliferation, of which the low concentration had negligible effect while the medium concentration showed obvious inhibitory effect [20]. Results showed that low dose of ZnO NPs could not effectively inhibit cell migration in wound healing assay, and the inhibition ability were generally enhanced with the increasing concentration of ZnO NPs (Fig. 2). We also found that the number of cells penetrating the transwell chamber were significantly decreased when compared to that in the control group (Fig. 3a–d). These results indicated that ZnO NPs have the potential to inhibit OS metastasis with suitable dose administration.

3.3. ZnO NPs inhibit EMT in OS cells

In malignant tumors, EMT is commonly considered as a vital process for tumor metastasis. During the process of EMT, levels of epithelial markers, like E-cadherin and tight junction protein zonula occluden-l

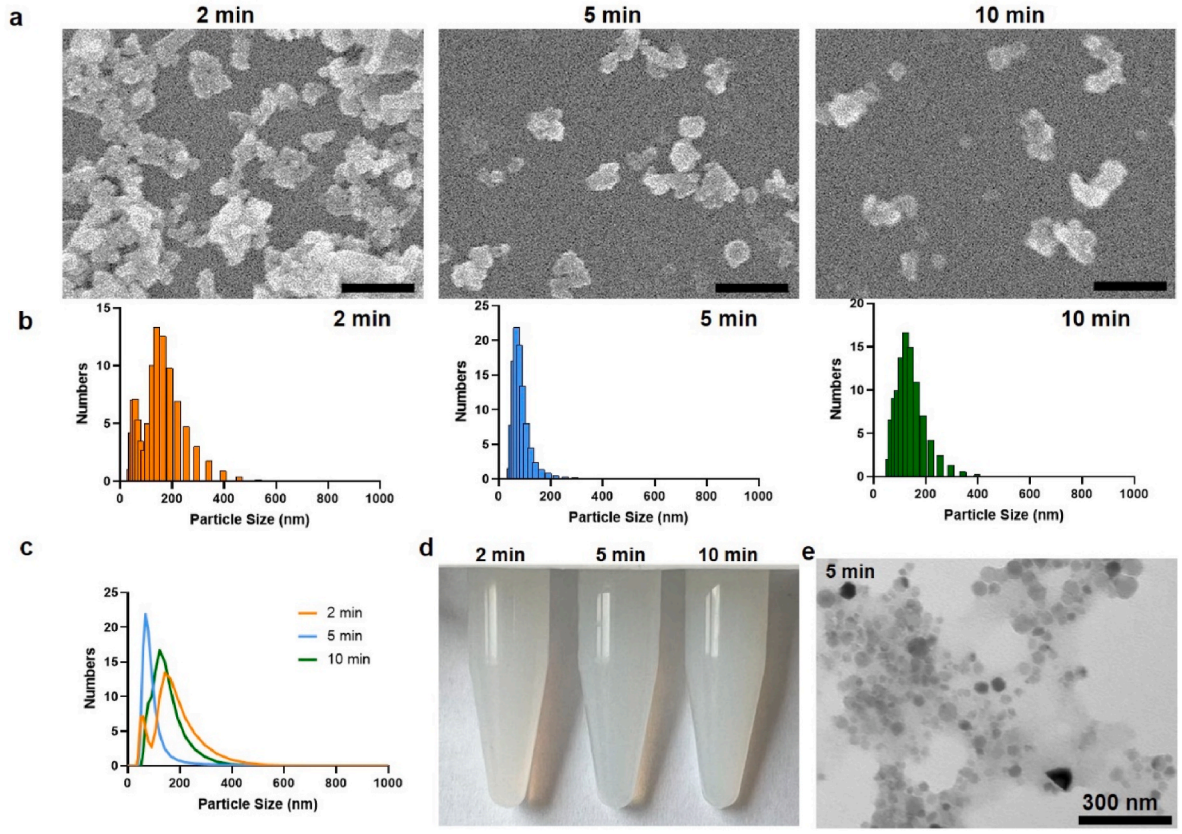

Fig. 1. Morphologies of ZnO NPs with different ultrasonic treatments. (a) Representative SEM images of ZnO NPs after ultrasonic treatment for 2, 5, 10 min (Scale bar: 300 nm). (b, c) Particle sizes and distribution of ZnO NPs after ultrasonic treatment for 2, 5, 10 min. (d) Representative image of ZnO NPs (1 mg/ml) after ultrasonic treatment for 2, 5, 10 min. (e) Representative TEM images of ZnO NPs after ultrasonic treatment for 5 min.

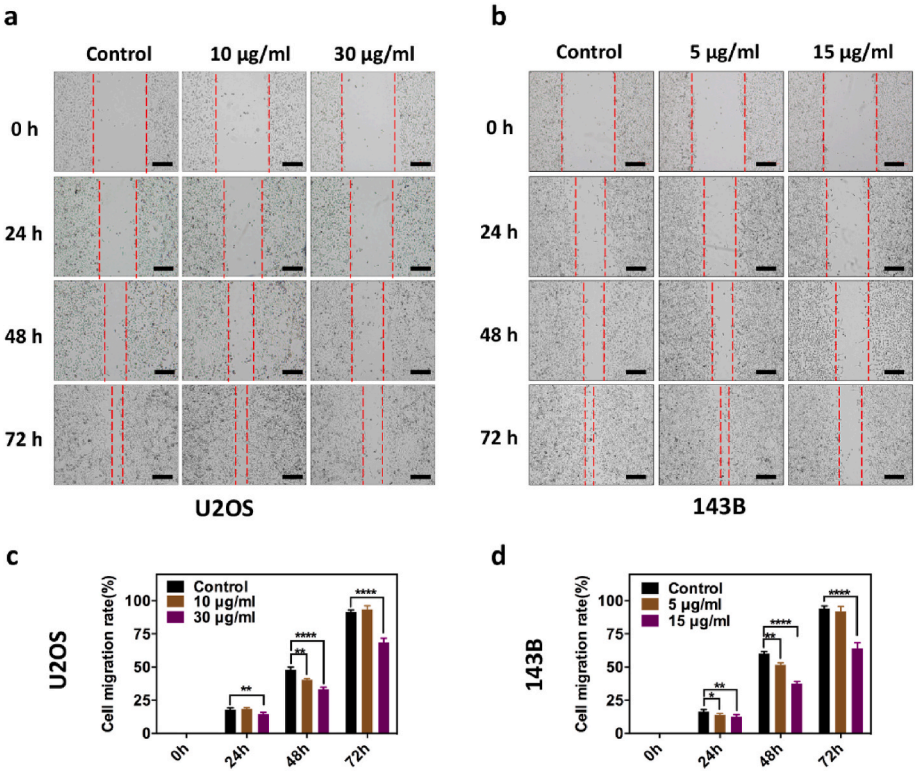

Fig. 2. Effect of ZnO NPs on cell migration in OS cells. (a, b) Wound healing assay showed that the distance of cell migration in U2OS and 143B cells were both decreased after ZnO NPs treatment in a dose and time-dependent manner (Scale bar: 100 μm). (c, d) Cell migration rates in (a, b) were plotted by respective histogram. Each bar represents the mean ± SD of three independent observations. (*$p < 0.05$, **$p < 0.01$, ***$p < 0.001$, and ****$p < 0.0001$).

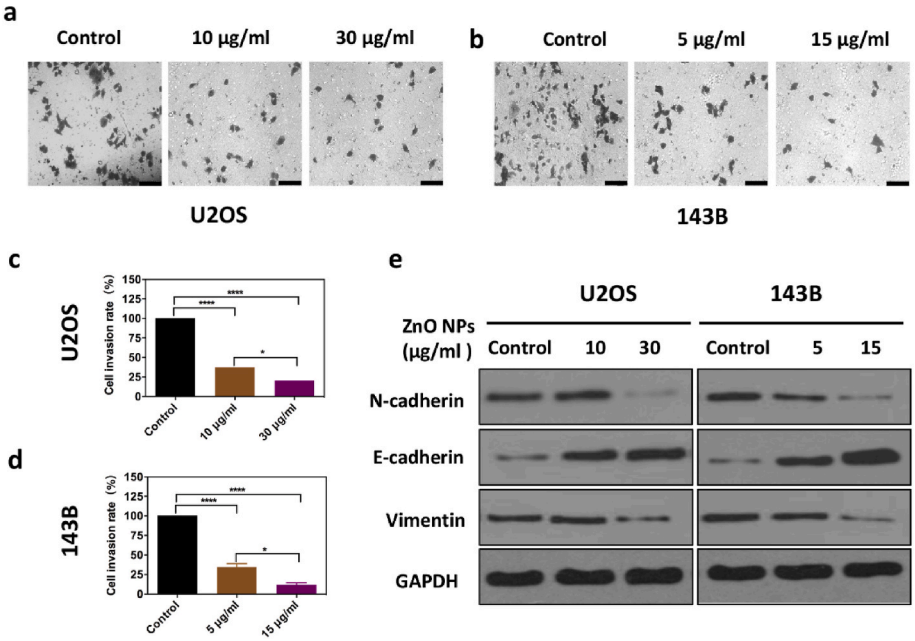

Fig. 3. Effect of ZnO NPs on cell invasion and EMT in OS cells. (a, b) The number of U2OS and 143B cell invasion were both significantly decreased after ZnO NPs treatment (Scale bar: 100 μm). (c, d) U2OS and 143B cell invasion rates in (a, b) were plotted by respective histogram. (e) ZnO NPs significantly downregulated mesenchymal phenotype proteins (vimentin and N-cadherin), and upregulated epithelial phenotype protein (E-cadherin) expression in U2OS and 143B OS cells. Each bar represents the mean ± SD of three independent observations. (*$p < 0.05$, **$p < 0.01$, ***$p < 0.001$, and ****$p < 0.0001$).

(ZO-1), are downregulated, and correspondingly levels of mesenchymal proteins, such as vimentin and N-cadherin, are upregulated, resulting in epithelial cell polarity lost, looser intercellular connections and cytoskeletal protein recombination, which eventually enable tumor invasion and metastasis [24]. Therefore, targeting EMT is a hot topic in tumor treatment. In general, EMT is believed to be a metastasis-related step in epithelial tissue-derived tumors. However, in recent years, studies have also found that EMT plays an important role in interstitial tissue-derived OS metastasis [25–27]. More and more studies verified that the process of EMT in OS is the main process for many drugs [28]. In this study, we found that both low and medium concentrations of ZnO NPs can significantly downregulate vimentin and N-cadherin and upregulate E-cadherin in OS cells (Fig. 3e), suggesting that ZnO NPs may target the process of EMT to inhibit OS cell metastasis.

3.4. RNA-Seqs analysis of ZnO NP-treated OS cells

Total RNA of 143B cells before and after ZnO NPs treatment were collected for RNA-Seqs analysis. Our results showed that the number of DEGs treated with ZnO NPs was 2768 (1628 genes were up-regulated and 916 genes were down-regulated) (Fig. 4a–c). KEGG pathway enrichment analysis found that the Wnt and HIF-1signaling pathway were significantly enriched (Fig. 4d). Our previous study has verified that HIF-1 pathway was activated in ZnO NP-treated OS cells, and related DEGs mRNA expression in the Wnt signaling pathway after ZnO NPs treatment were also verified by qPCR. We found that compared to the control group, Wnt4, FZD7, β-catenin and c-Myc mRNA transcription activity in ZnO NP-treated group were significantly upregulated (Fig. 4e).

Those above results confirmed that the Wnt signaling pathway was activated in ZnO NP-treated OS cells. However, our results unexpectedly detected that ZnO NPs significantly downregulated β-catenin expression in U2OS and 143B OS cells in a dose-dependent manner, and further observed obvious downregulation in cytoplasm and even rarely to be detected in nucleus in 143B OS cells (Fig. 4f and g). Based on above, we

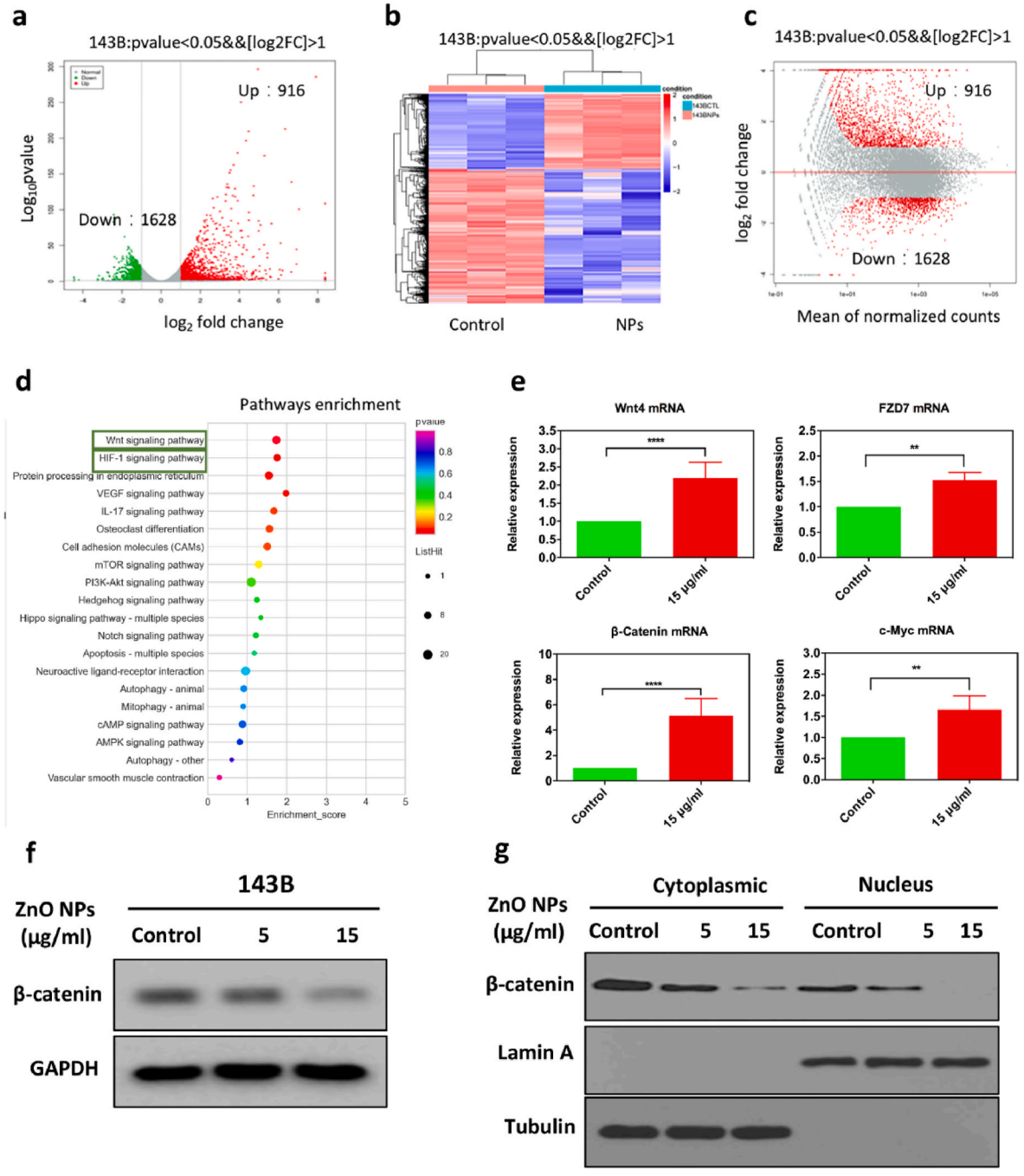

Fig. 4. Differentially expressed genes (DEGs, a cutoff value of [log2FC] >1 and P < 0.05) were analyzed by RNA-Seq in ZnO NPs-treated (15 μg/ml) 143B cells compared to the untreated control group. DEGs were exhibited by (a) volcano plot, (b) heatmap, and (c) MA plot. (d) Pathways enrichment of DEGs based on KEGG enrichment analysis was showed by bubble chart plot. (e) Genes expression in Wnt pathway detected by qPCR. (f) ZnO NPs significantly decreased total β-catenin expression in 143B OS cells in a dose-dependent manner. (g) ZnO NPs significantly decreased β-catenin expression both in cytoplasm and nucleus of 143B OS cells in a dose-dependent manner, especially in nucleus which was nearly undetectable. Each group was determined for triplicate times.

can infer that although ZnO NPs can upregulate β-catenin mRNA transcription, it also induces β-catenin protein degradation, which ultimately inhibit OS cell metastasis.

3.5. The role of key pathways verified in ZnO NPs-induced OS metastasis inhibition

Increasing evidences have shown that there is an intimate relationship between the autophagy and Wnt pathway [29,30]. For example, studies have reported that the Wnt pathway activation can negatively regulate autophagy by downregulating beclin-1 expression [31,32]. In contrast, other studies have also reported that the autophagy-related protein LC3B can bind the LC3-interacting region (LIR) of β-catenin to form the LC3B/β-catenin complex, ultimately resulting in β-catenin degradation in the autolysome [33]. In our previous study, we have confirmed that ZnO NPs induced OS cell death via HIF-1α/BNIP3/LC3B-mediated mitophagy pathway. Therefore, there might exist an intimate relationship between HIF-1α/BNIP3/LC3B-mediated mitophagy and the Wnt/β-catenin pathway in ZnO NP-treated OS.

Firstly, we used LiCl (a β-catenin activator), and ICG-001(a β-catenin inhibitor) to verify the function of the Wnt/β-catenin pathway in ZnO NP-induced OS metastasis inhibition. Our results showed that LiCl could significantly reverse the ZnO NP-induced OS cell proliferation, migration, invasion and EMT inhibition, while ICG-001 showed the reversed effect (Supplementary Fig. S3a; Fig. 5). We further evaluated the effect of $CoCl_2$ (a HIF-1 pathway activator) and YC-1 (a HIF-1 pathway inhibitor) on ZnO NP-induced OS cell metastasis inhibition. Our results also showed that $CoCl_2$ can further inhibit ZnO NP-induced OS cell proliferation, migration, and invasion, while YC-1 showed the opposite effect (Supplementary Figs. S3b, S4, S5). These above results suggested that both HIF-1α/BNIP3/LC3B-mediated mitophagy and the Wnt/β-catenin pathway played vital roles in regulating ZnO NP-induced OS metastasis inhibition.

3.6. Mechanism of β-catenin downregulation in ZnO NP-treated OS cells

Previous studies have reported that HIF-1α can compete with TCF-4 to combine with β-catenin, resulting in forming HIF-1α/β-catenin complex and promoting tumor cell proliferation and metastasis [33]. Therefore, it is generally believed that HIF-1α activation will upregulate β-catenin expression. However, our current study unexpectedly detected that ZnO NPs induced downregulation of β-catenin expression, which seemed to contradict with previous studies. In fact, researchers have verified that β-catenin can also bind to LC3B via its LIR to be degraded

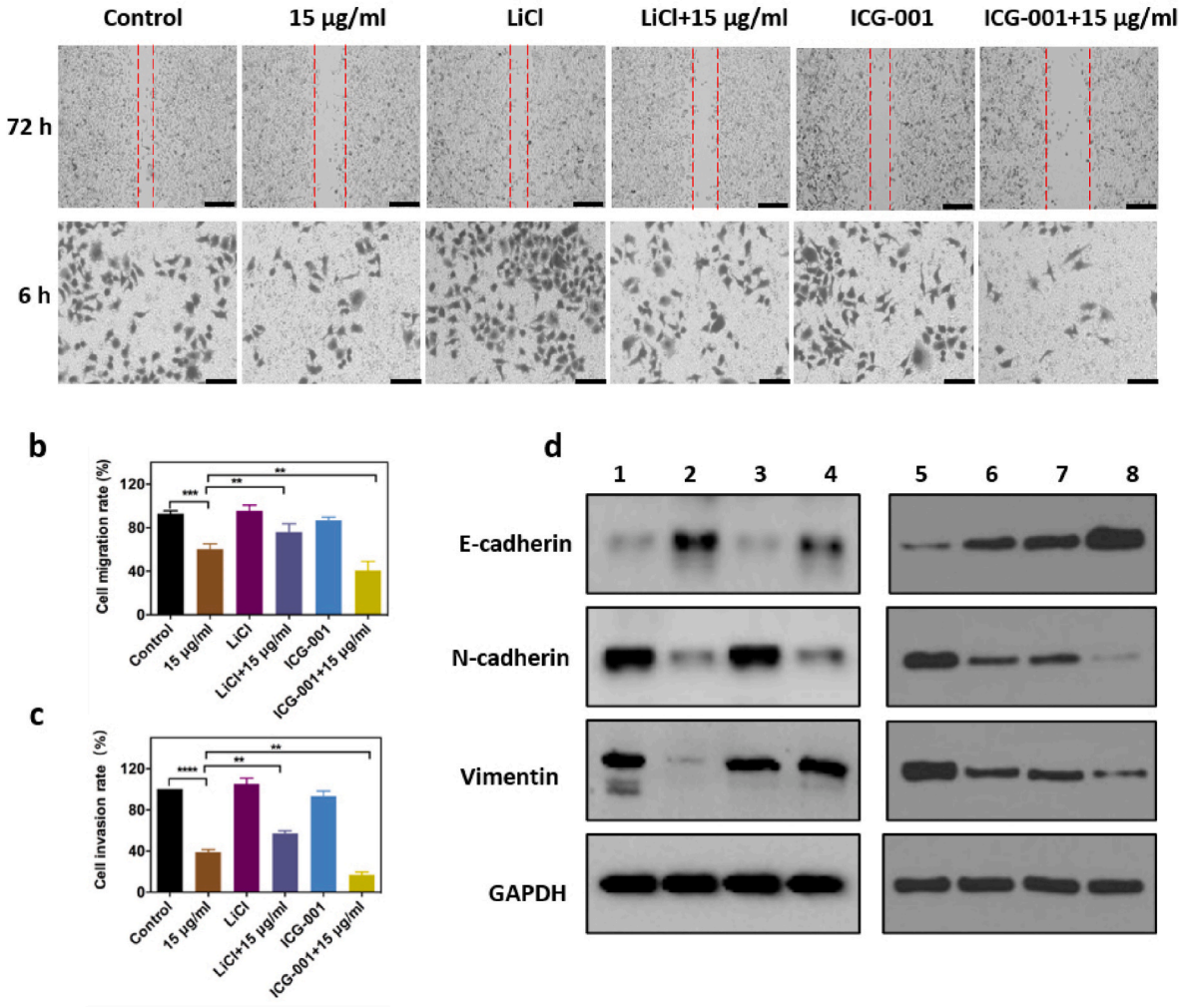

Fig. 5. ZnO NPs inhibited 143B OS cell migration, invasion and EMT by regulating Wnt/β-catenin pathway. (a) Wnt/β-catenin pathway activator LiCl (10 mM) reversed ZnO NPs-induced cell proliferation, migration, and invasion inhibition, while inhibitor ICG-001(10 μM) showed the opposite effect (Scale bar: 100 μm). (b–c) Cell migration and invasion rates in (a) were plotted by respective histogram. (d) Wnt/β-catenin pathway activator LiCl (10 mM) reversed ZnO NPs-induced mesenchymal phenotype proteins (vimentin and N-cadherin) downregulation, and epithelial phenotype protein (E-cadherin) expression upregulation, while the inhibitor ICG-001(10 μM) showed the opposite effect. Each bar represents mean ± SD of three independent observations. *$p < 0.05$, **$p < 0.01$, ***$p < 0.001$, and ****$p < 0.0001$. 1–8 respectively represent: Control, 15 μg/ml, LiCl, LiCl +15 μg/ml, Control, 15 μg/ml, IC G-001, ICG-001 + 15 μg/ml.

by a proteasome-independent autophagy pathway [31]. Therefore, we speculated that the seemingly contradictory phenomenon that ZnO NPs induced HIF-1α upregulation but β-catenin downregulation may be the result of HIF-1α/BNIP3/LC3B-mediated mitophagy degradation pathway.

To verify the above assumption, we firstly used TEM detected the changes of cell ultrastructure after ZnO NPs treatment. TEM directly observed that the endocytosis of NPs and autophagosome containing mitochondria (Fig. 6a). We further found that pan-autophagy inhibitor 3 MA rather than pan-proteasome inhibitor MG132 succeed to reverse ZnO NP-induced cell proliferation inhibition (Fig. 6b). Correspondingly, we detected that 3 MA but not MG132 successfully reversed ZnO NPs-induced β-catenin degradation (Fig. 6c). Furthermore, we used siRNA to verify the role of autophagy in ZnO NP-induced β-catenin degradation. Results showed that LC3B siRNA obviously reversed ZnO NP-induced cell proliferation inhibition and β-catenin downregulation (Fig. 6d–f).

Moreover, we conducted immunofluorescence confocal and Co-IP assays to clarify the relationship between β-catenin and LC3B in OS cells. Immunofluorescence result observed that co-localization of β-catenin and LC3B was significantly enhanced after ZnO NPs treatment (Fig. 7a). Co-IP further detected that LC3B immunoprecipitated with β-catenin was enhanced by ZnO NPs treatment (Fig. 7b). Based on above all, we can conclude that ZnO NPs activated HIF-1α/BNIP3/LC3B-mediated mitophagy in OS cells, which can degrade β-catenin via being bonded and dragged by LC3B, resulting in OS metastasis inhibition.

3.7. Zn^{2+} released from ZnO NPs triggers anti-osteosarcoma biological effect

Previous studies have showed that low concentration of intercellular Zn^{2+} can promote the cancer occurrence and development, but high concentration reversely show a killing effect [34,35]. We also proved that OS proliferation, autophagy and apoptosis inhibition were mediated by Zn^{2+} releasing from ZnO NPs [20]. In this study, we further observed that zinc chelators EDTA can significantly reduce the concentration of intracellular Zn^{2+}, reverse the inhibition of OS cell proliferation, migration and invasion, block HIF-1a upregulation and β-catenin downregulation (Supplementary Fig. S6; Fig. 8), which suggested that it is the Zn^{2+} released from ZnO NPs triggered HIF-1 and Wnt pathway activation to inhibit OS cell metastasis by HIF-1α/BNIP3/LC3B-mediated mitophagy degradation pathway induced degradation of β-catenin (Fig. 9).

3.8. ZnO NPs inhibit tibia orthotopic OS growth and lung metastasis

The lung is the most common organ of OS metastasis. Once it occurs, the survival time of OS patients will be significantly reduced. Therefore, it is very important to further evaluate drugs with definite tumor killing effect whether can also effectively inhibit OS metastasis. In this study, 143B cells were used to construct tibia orthotopic OS model. After ZnO NPs, ICG-001 or ZnO NPs + ICG-001 treatment, we observed that tumor volumes and weight in the intervention groups obviously decreased after two-week treatment, especially in ZnO NPs + ICG-001 group (Fig. 10a–c), which showed significant difference compared with ZnO NPs or ICG-001 alone groups.

Correspondingly, Tunel and IHC staining detected that apoptosis ratio obviously increased and ki-67 expression significantly decreased in the ZnO NPs and ZnO NPs + ICG-001 groups, especially in ZnO NPs + ICG-001 group (Fig. 10d). Meantime, the gross and microscopic observations found that numbers of lung metastatic nodules in the intervention groups were obviously reduced compared to the control group,

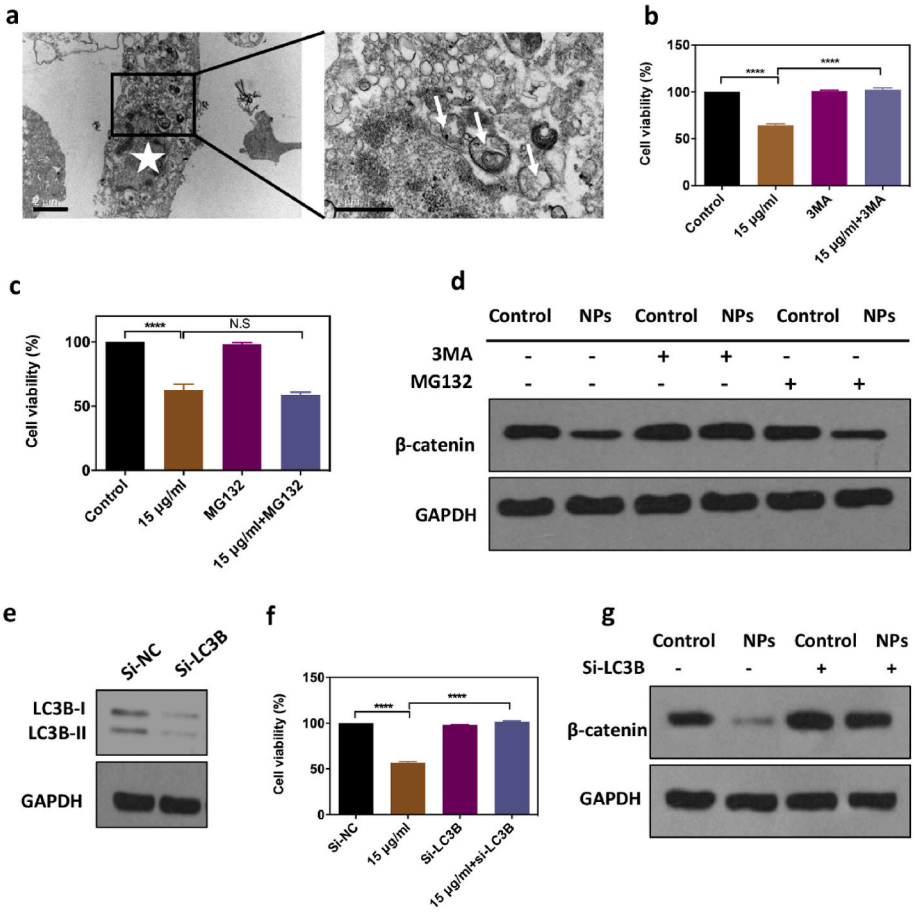

Fig. 6. β-catenin was degraded in a protease-independent mitophagy pathway in ZnO NPs-treated 143B OS cells. (a) Left: Changes of Cell morphology after ZnO NPs treatment observed by TEM (Scale bar: 2 μm). Right: a further magnification of the small black square of left, the white star and arrows respectively represent destruction of nucleus and autophagosomes containing mitochondria (Scale bar: 1 μm). (b, c) Pan-autophagy inhibitor 3 MA (10 mM) significantly succeed to rescue ZnO NP-induced cell proliferation but not protease inhibitor MG132. (d) Pan-autophagy inhibitor 3 MA (10 mM) significantly reversed ZnO NP-induced β-catenin degradation but not MG132 did (100 nM). (e) LC3B siRNA successfully knockdown LC3B protein expression. (f, g) LC3B siRNA reversed ZnO NPs induced cell proliferation inhibition and β-catenin downregulation. Each bar represented the mean ± SD of three independent observations. (*$p < 0.05$, **$p < 0.01$, ***$p < 0.001$, and ****$p < 0.0001$; NPs refer to ZnO NPs with a concentration of 15 μg/ml).

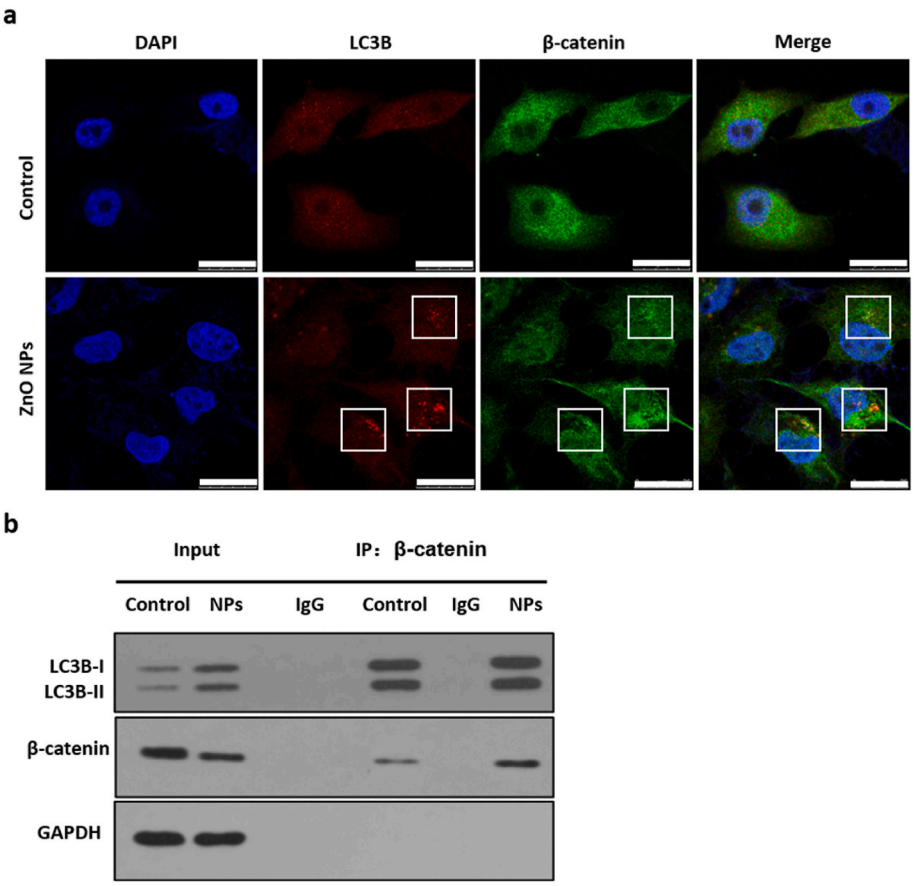

Fig. 7. Interaction between LC3B and β-catenin was enhanced by ZnO NPs treatment in 143B OS cells. (a) Immunofluorescence confocal observed that there existed a co-localization of β-catenin and LC3B after ZnO NPs treatment compared to the control group (Scale bar: 25 μm). (b) Co-IP confirmed that there existed an interaction between β-catenin and LC3B, which can be significantly enhanced by ZnO NPs treatment. NPs represented as ZnO NPs with a concentration of 15 μg/ml. Each group was determined for triplicate times.

especially in the ZnO NPs + ICG-001 group (Fig. 10e–h). During this process, we did not observe loss of body weight and obvious damage to important organs in the treated groups compared to the control group (Supplementary Figs. S7 and 8).

In addition, we further observed that mice (3/5) in the ZnO NPs + ICG-001 group survived for over 50 days, which was significantly longer than that in other groups (Fig. 10i). These above results confirmed that ZnO NPs combined with targeting Wnt/β-catenin pathway can exert synergistic inhibitory effects on OS growth and lung metastases with good biosafety.

3.9. The effect of ZnO NPs on β-catenin expression in OS cells

To confirm the clinical relevance of this study, we further evaluate β-catenin in human samples. Related studies have reported that proportion of β-catenin expression in OS tissues can reach 50%–70%, which is obviously higher than that in normal bone tissues [36,37]. In this study, we used TMA to observe and evaluate the characteristic of β-catenin expression in OS tissues. Results showed that positive β-catenin expression in OS tissues was 51.2% (40 of 78), and widely distributed in the cell membrane (25/78), cytoplasm (34/78), and nucleus (9/78) (Fig. 11a–d), which was consistent with our in vitro results. The results confirmed the potential of β-catenin as a target in osteosarcoma metastasis inhibition and suggested that the ZnO NPs therapy provides promising options for clinical OS therapy.

4. Conclusions

This study focused on the effect and regulatory mechanism of bioactive ZnO NPs on OS metastasis. Series of in vitro and in vivo experiments proved that Zn^{2+} released from ZnO NPs could trigger HIF-1 and Wnt pathway activation to inhibit OS cell metastasis by HIF-1α/BNIP3/LC3B-mediated mitophagy degradation pathway induced degradation of β-catenin. The in vivo results also confirmed that ZnO NPs combined with blocking Wnt/β-catenin pathway showed a synergistic effect on OS growth and lung metastasis. Thus, ZnO NPs may be used as an adjunctive therapeutic agent together with ICG-001. Our current study further explored a novel mechanism of ZnO NP-induced OS metastasis inhibition, providing a solid theoretical and practical foundation for the future application of ZnO NPs in anti-osteosarcoma metastasis. OS tissue microarray (TMA) from OS patients also detected higher β-catenin expression, which further indicated a far-reaching potential of ZnO NPs in clinical OS treatment with metastasis.

Ethics approval and consent to participate-BAM

All animal procedures were performed in accordance with the Guidelines for Care and Use of Laboratory Animals of Beijing Jishuitan Hospital and approved by the Animal Ethics Committee of the Beijing Jishuitan Hospital.

Affidavit of Approval of Animal Ethics and Welfare

Approval No.: Beijing Jishuitan Hospital Ethics Review Committee Animal Experiment Review Form No. 202103-03.

Program: Construct and Mechanism Study of Bone Tumor-Responsive Multi-Functional Polycationic circRNA Carriers.

Name of Principal Investigator: Da-Fu Chen.

Department: Beijing Research Institute of Traumatology and Orthopaedics.

Sponsor**:** National Natural Science Foundation of China.

Period of Protocol: 2021.03.05–2022.03.04.

Submissions for Review

1.Application form for Ethical Review of Animal Experiments.

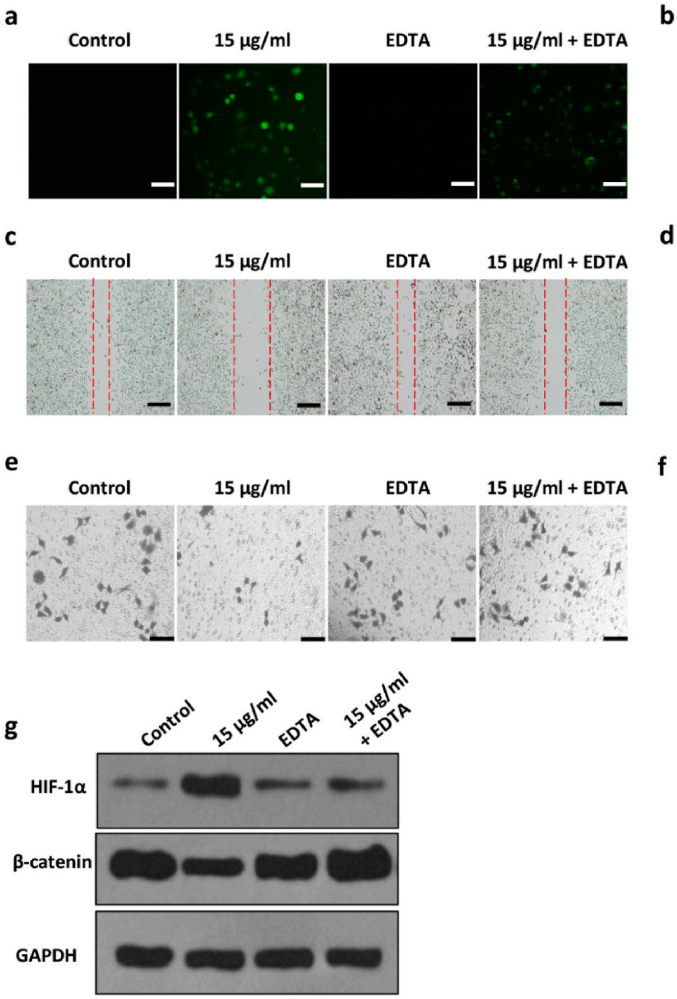

Fig. 8. ZnO NPs activated HIF-1 and Wnt pathway, inhibited migration, and invasion in 143B OS cells were triggered by Zn^{2+}. (a, b) EDTA significantly decreased the level of intercellular Zn^{2+} under ZnO NPs treatment observed by immunofluorescence microscope and ICP-MS (Scale bar:100 μm). (c–f) EDTA reversed cell migration and invasion induced by ZnO NPs (Scale bar:100 μm). (g) EDTA significantly reversed ZnO NP-induced HIF-1α upregulation and β-catenin downregulation. Each bar represented the mean ± SD of three independent observations. (*$p < 0.05$, **$p < 0.01$, ***$p < 0.001$, and ****$p < 0.0001$).

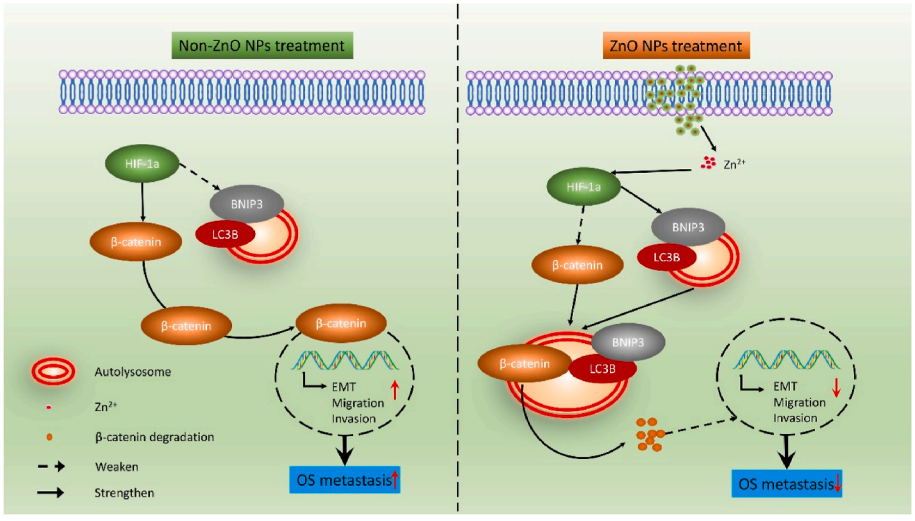

Fig. 9. Mechanism of ZnO NPs-induced OS cell metastasis inhibition. Under non-ZnO NPs treatment, HIF-1α/β-catenin activation pathway is stronger than HIF-1α-BNIP3/LC3B/β-catenin degradation pathway, resulting in β-catenin upregulation and translocating into nucleus to promote OS EMT and metastasis. Under ZnO NPs treatment, HIF-1α/BNIP3/LC3B/β-catenin degradation pathway is stronger than HIF-1α/β-catenin activation pathway, resulting in β-catenin degradation to inhibit OS EMT and metastasis.

2.Application Format for Ethical Approval for Research Involving Animals.

Results of inspection

According to the regulations on the Management of Experimental Animals and other regulations, the ethics Committee has approved the Animal experiments.

Chairman: Xieyuan Jiang.

CRediT authorship contribution statement

Guanping He: Project administration, Methodology, Investigation, Writing – original draft. **Jing-Jun Nie:** Project administration,

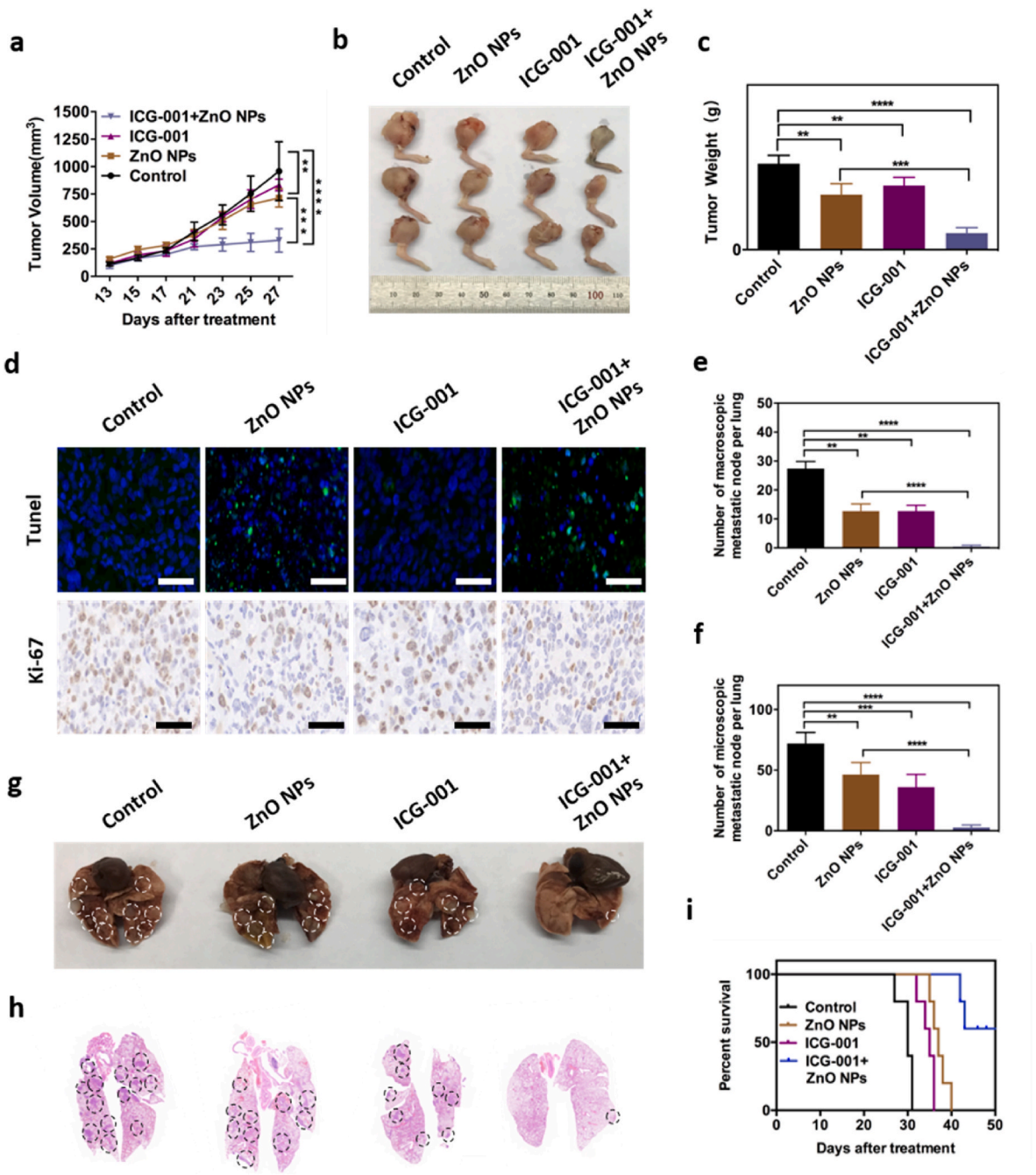

Fig. 10. The effect of ZnO NPs combined with ICG-001 on 143B tibial orthotopic OS growth and lung metastasis. (a) Tumor growth curve during the therapy. (b, c) Representative images of OS tibial orthotopic tumor and tumor weight at day 27 after corresponding treatments. (d) Representative TUNEL staining and IHC staining show the apoptosis ratio and ki-67 expression in tumor tissues after different treatments (Scale bar: 200 μm). (g, h) The gross and microscopic observations showed the inhibitory effect of different treatments on OS lung metastasis (typical nodules of metastasis were circled). (e, f) Number of lung nodes in (g, h) were plotted by respective histogram. (i) Survival time after different treatments. Control group, PBS; ZnO NPs group, 5 mg/kg ZnO NPs; ICG-001 group, 50 mg/kg ICG-001; ICG-001 + ZnO NPs group, 50 mg/kg ICG-001 and 5 mg/kg ZnO NPs. Each bar represents mean ± SD of three independent observations. (*$p < 0.05$, ***$p < 0.001$, and ****$p < 0.0001$).

Methodology, Investigation, Writing – original draft. **Xiao Liu:** Project administration, Methodology, Investigation, Writing – original draft. **Zihao Ding:** Data curation, experimental operation. **Peng Luo:** Data curation, experimental operation. **Yu Liu:** Resources, Data curation, Supervision. **Bo-Wen Zhang:** Resources, Data curation, Supervision. **Renxian Wang:** Resources, Data curation, Supervision. **Xiaoguang Liu:** Supervision, Conceptualization, Writing – review & editing, Funding acquisition, All authors reviewed the paper and approved the submitted and published versions of the paper. **Yong Hai:** Supervision, Conceptualization, Writing – review & editing, Funding acquisition, All authors reviewed the paper and approved the submitted and published versions of the paper. **Da-Fu Chen:** Supervision, Conceptualization, Writing – review & editing, Funding acquisition, All authors reviewed the paper and approved the submitted and published versions of the paper.

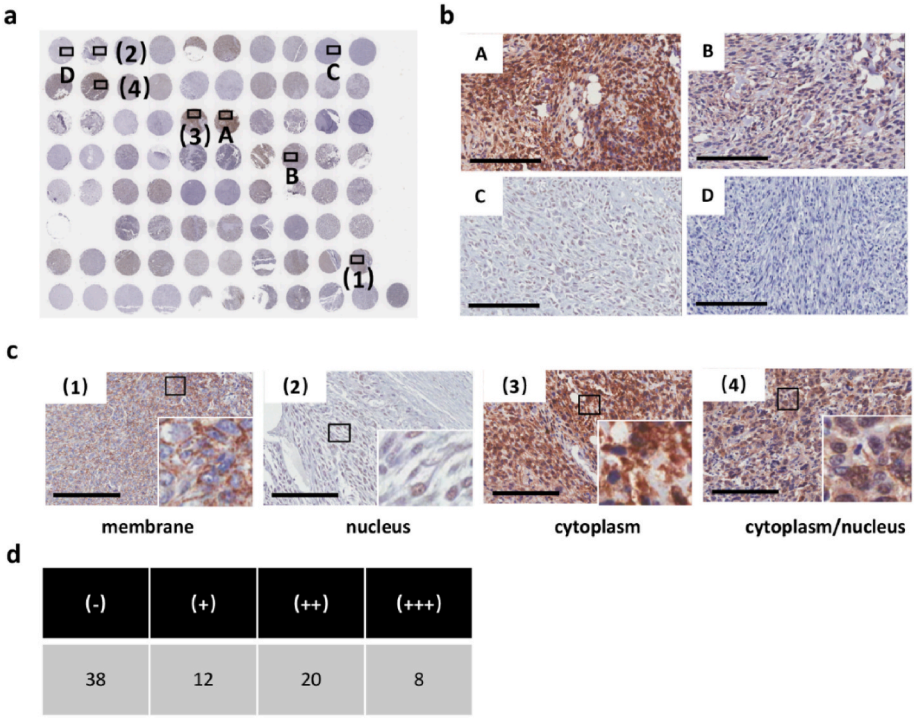

Fig. 11. Characteristics of β-catenin expression in human OS patient tissues. (a) Tissue microarrays (TMA) of OS tissues. (b) Differential β-catenin expression in TMA of human OS tissues (Scale bar: 200 μm). (c) Intracellular distribution of β-catenin expression in TMA of human OS tissues (Scale bar: 200 μm); Inset: a further magnification of the small black square. (d) Statistical analysis of differential β-catenin expression in TMA of human OS tissues.

Declaration of competing interest

The authors declare no conflict of interest.

Acknowledgements

This work was supported in part by Beijing Natural Science Foundation (7192226, 7222011), Beijing Chao-Yang Hospital Golden Seeds Foundation (CYJZ202148), National Key Research and Development Program (2021YFC2400500), National Natural Science Foundation of China (51903013, 51973021, 51932002, 52173275), Beijing Hospitals Authority Youth Programme (QML20210402), and the Beijing Municipal Health Commission (PXM 2020_026275_000002, BMHC-2021-6, BMHC-2019-9). We feel grateful to the Medical Research Center of Peking University Third Hospital for providing technical support.

Appendix A. Supplementary data

Supplementary data to this article can be found online at https://doi.org/10.1016/j.bioactmat.2022.05.006.

References

[1] L. Mirabello, R.J. Troisi, S.A. Savage, Osteosarcoma incidence and survival rates from 1973 to 2004: data from the surveillance, epidemiology, and end results program, Cancer 115 (2009) 1531–1543.
[2] J.S. Whelan, L.E. Davis, Osteosarcoma, chondrosarcoma, and chordoma, J. Clin. Oncol. 36 (2018) 188–193.
[3] L. Kager, G. Tamamyan, S. Bielack, Novel insights and therapeutic interventions for pediatric osteosarcoma, Future Oncol. 13 (2017) 357–368.
[4] Z. Deng, S. Bi, M. Jiang, S. Zeng, Endogenous H2S-activated orthogonal second near-infrared emissive nanoprobe for in situ ratiometric fluorescence imaging of metformin-induced liver injury, ACS Nano 15 (2021) 3201–3211.
[5] C. Meazza, P. Scanagatta, Metastatic osteosarcoma: a challenging multidisciplinary treatment, Expert Rev. Anticancer Ther. 16 (2016) 543–556.
[6] Y. Okinaka, M. Takahashi, Osteosarcoma of the maxilla: report of a case and review of the literature concerning metastasis, J. Oral Maxillofac. Surg. 55 (1997) 1177–1181.
[7] L.E. Shi, Z.H. Li, W. Zheng, Y.F. Zhao, Y.F. Jin, Z.X. Tang, Synthesis, antibacterial activity, antibacterial mechanism and food applications of ZnO nanoparticles: a review, Food Addit. Contam. Part A Chem Anal Control Expo Risk Assess 31 (2014) 173–186.
[8] J.W. Rasmussen, E. Martinez, P. Louka, D.G. Wingett, Zinc oxide nanoparticles for selective destruction of tumor cells and potential for drug delivery applications, Expet Opin. Drug Deliv. 7 (2010) 1063–1077.
[9] J. Wang, S. Gao, S. Wang, Z. Xu, L. Wei, Zinc oxide nanoparticles induce toxicity in CAL 27 oral cancer cell lines by activating PINK1/Parkin-mediated mitophagy, Int. J. Nanomed. 13 (2018) 3441–3450.
[10] A.M. Leidal, B. Levine, J. Debnath, Autophagy and the cell biology of age-related disease, Nat. Cell Biol. 20 (2018) 1338–1348.
[11] S. Shimizu, S. Honda, S. Arakawa, H. Yamaguchi, Alternative macroautophagy and mitophagy, Int. J. Biochem. Cell Biol. 50 (2014) 64–66.
[12] J.P. Piret, D. Mottet, M. Raes, C. Michiels, Is HIF-1α a pro- or an anti-apoptotic protein? Biochem. Pharmacol. 64 (2002) 889–892.
[13] N.M. Mazure, J. Pouyssegur, Hypoxia-induced autophagy: cell death or cell survival? Curr. Opin. Cell Biol. 22 (2010) 177–180.
[14] G. He, X. Pan, X. Liu, Y. Zhu, Y. Ma, C. Du, X. Liu, C. Mao, HIF-1α-Mediated mitophagy determines ZnO nanoparticle-induced human osteosarcoma cell death both in vitro and in vivo, ACS Appl. Mater. Interfaces 12 (2020) 48296–48309.
[15] Y. Cai, T. Cai, Y. Chen, Wnt pathway in osteosarcoma, from oncogenic to therapeutic, J. Cell. Biochem. 115 (2014) 625–631.
[16] F. Guo, H. Wang, M. Jiang, Q. Yang, Q. Xiang, H. Zhou, X. Hu, K. Hao, J. Yang, H. Cao, Z. Shen, TDP-43 induces EMT and promotes hepatocellular carcinoma metastasis via activating Wnt/β-catenin signaling pathway, Am. J. Cancer Res. 10 (2020) 3285–3301.
[17] Y. Zhang, X. Wang, Targeting the Wnt/β-catenin signaling pathway in cancer, J. Hematol. Oncol. 13 (2020) 165.
[18] S. Mehta, A. Nijhuis, T. Kumagai, J. Lindsay, A. Silver, Defects in the adherens junction complex (E-cadherin/β-catenin) in inflammatory bowel disease, Cell Tissue Res. 360 (2015) 749–760.
[19] Z.Y. Long, Y. Lu, M. Li, G. Chen, L. Shi, X. Xiao, Y. Bai, H.M. Zhang, Z. Wang, Effective treatment of anlotinib in giant delayed pulmonary metastasis of osteosarcoma: a case report and literature review, Ann. Palliat. Med. 10 (2021) 7073–7082.
[20] G. He, Y. Ma, Y. Zhu, L. Yong, X. Liu, P. Wang, C. Liang, C. Yang, Z. Zhao, B. Hai, X. Pan, Z. Liu, X. Liu, C. Mao, Cross talk between autophagy and apoptosis contributes to ZnO nanoparticle-induced human osteosarcoma cell death, Adv. Healthc. Mater. 7 (2018), e1800332.
[21] X. Pan, G. He, B. Hai, Y. Liu, L. Bian, L. Yong, H. Zhang, C. Yang, C. Du, T. Mao, Y. Ma, F. Jia, X. Dou, S. Zhai, X. Liu, VPS34 regulates dynamin to determine the endocytosis of mitochondria-targeted zinc oxide nanoparticles in human osteosarcoma cells, J. Mater. Chem. B 9 (2021) 2641–2655.
[22] M. Milanovic, D.N.Y. Fan, D. Belenki, J.H.M. Däbritz, Z. Zhao, Y. Yu, J.R. Dörr, L. Dimitrova, D. Lenze, I.A. M Barbosa, M.A. Mendoza-Parra, T. Kanashova,

M. Metzner, K. Pardon, M. Reimann, A. Trumpp, B. Dörken, J. Zuber, H. Gronemeyer, M. Hummel, G. Dittmar, S. Lee, C.A. Schmitt, Senescence-associated reprogramming promotes cancer stemness, Nature 553 (2018) 96–100.
[23] P.P. Kushwaha, S. Gupta, A.K. Singh, A.K. Singh, S. Kumar, Emerging role of migration and invasion enhancer 1 (MIEN1) in cancer progression and metastasis, Front. Oncol. 9 (2019) 868.
[24] M.A. Nieto, R.Y. Huang, R.A. Jackson, J.P. Thiery, EMT: 2016, Cell 166 (2016) 21–45.
[25] G. Yang, J. Yuan, K. Li, EMT transcription factors: implication in osteosarcoma, Med. Oncol. 30 (2013) 697.
[26] M. Ruh, M.P. Stemmler, I. Frisch, K. Fuchs, R. Roey, J. Kleemann, M. Roas, H. Schuhwerk, R.L. Eccles, A. Agaimy, D. Baumhoer, G. Berx, F. Müller, T. Brabletz, S. Brabletz, The EMT transcription factor ZEB1 blocks osteoblastic differentiation in bone development and osteosarcoma, J. Pathol. 254 (2021) 199–211.
[27] Y.X. Peng, B. Yu, H. Qin, L. Xue, Y.J. Liang, Z.X. Quan, EMT-related gene expression is positively correlated with immunity and may be derived from stromal cells in osteosarcoma, PeerJ 8 (2020) e8489.
[28] Z.X. Chong, S.K. Yeap, W.Y. Ho, Unraveling the roles of miRNAs in regulating epithelial-to-mesenchymal transition (EMT) in osteosarcoma, Pharmacol. Res. 172 (2021) 105818.
[29] C. Perez-Plasencia, E. Lopez-Urrutia, V. Garcia-Castillo, S. Trujano-Camacho, C. López-Camarillo, A.D. Campos-Parra, Interplay between autophagy and Wnt/β-catenin signaling in cancer: therapeutic potential through drug repositioning, Front. Oncol. 10 (2020) 1037.
[30] S. Lorzadeh, L. Kohan, S. Ghavami, N. Azarpira, Autophagy and the Wnt signaling pathway: a focus on Wnt/β-catenin signaling, Biochim. Biophys. Acta Mol. Cell Res. 1868 (2021) 118926.
[31] X.X. Xiong, D.X. Hu, L. Xu, H. Lin, Y. Zhang, C.Y. Li, X.Q. Chen, Selective 14-3-3γ upregulation promotes Beclin-1-LC3-autophagic Influx viaβ-catenin interaction in starved neurons in vitro and in vivo, Neurochem. Res. 44 (2019) 849–858.
[32] T.M. Nguyen, I.V. Subramanian, X. Xiao, G. Ghosh, P. Nguyen, A. Kelekar, S. Ramakrishnan, Endostatin induces autophagy in endothelial cells by modulating Beclin 1 and β-catenin levels, J. Cell Mol. Med. 13 (2009) 3687–3698.
[33] H. Wu, X.X. Lu, J.R. Wang, T.Y. Yang, X.M. Li, X.S. He, Y. Li, W.L. Ye, Y. Wu, W. J. Gan, P.D. Guo, J.M. Li, TRAF6 inhibits colorectal cancer metastasis through regulating selective autophagic CTNNB1/β-catenin degradation and is targeted for GSK3B/GSK3β-mediated phosphorylation and degradation, Autophagy 15 (2019) 1506–1522.
[34] W. Maret, Zinc in cellular regulation: the nature and significance of “Zinc Signals”, Int J Mol Sci 18 (2017) 2285.
[35] R.B. Franklin, L.C. Costello, The important role of the apoptotic effects of zinc in the development of cancers, J. Cell. Biochem. 106 (2009) 750–757.
[36] R.C. Haydon, A. Deyrup, A. Ishikawa, R. Heck, W. Jiang, L. Zhou, T. Feng, D. King, H. Cheng, B. Breyer, T. Peabody, M.A. Simon, A.G. Montag, T.C. He, Cytoplasmic and/or nuclear accumulation of the β-catenin protein is a frequent event in human osteosarcoma, Int. J. Cancer 102 (2002) 338–342.
[37] Z. Deng, G. Niu, L. Cai, R. Wei, X. Zhao, The prognostic significance of CD44V6, CDH11, and β-catenin expression in patients with osteosarcoma, BioMed Res. Int. 2013 (2013) 496193.